Accepted Author Manuscript (AAM)

Article Title: Insights into hydrodynamic and operational conditions for scalable hydrogen peroxide electrosynthesis applications

Authors: Robson da Silva Souto, Larissa Pinheiro de Souza, Paulo Jorge Marques Cordeiro Junior, Bruno Ramos, Antônio Carlos Silva Costa Teixeira, Robson da Silva Rocha, and Marcos Roberto de Vasconcelos Lanza

DOI: http://dx.doi.org/10.1021/acs.iecr.3c02139

Journal: *Industrial & Engineering Chemistry Research*

Received date: 26 July 2023
Revised date: 31 August 2023
Accepted date: 10 September 2023

Insights into hydrodynamic and operational conditions for scalable hydrogen peroxide electrosynthesis applications

Robson da Silva Souto[1*], Larissa Pinheiro de Souza[2], Paulo Jorge Marques Cordeiro Junior[1], Bruno Ramos[2], Antônio Carlos Silva Costa Teixeira[2], Robson da Silva Rocha[3], and Marcos Roberto de Vasconcelos Lanza[1*]

[1]*São Carlos Institute of Chemistry, University of São Paulo, 13560-970, São Carlos, SP, Brazil*

[2]*Research Group in Advanced Oxidation Processes (AdOx), Department of Chemical Engineering, Polytechnic School, University of São Paulo, 05508-010, São Paulo, Brazil*

[3]*School of Engineering of Lorena-EEL/USP, Municipal Road of Campinho S/N, CEP 12602-810, Lorena, São Paulo, Brazil*

*Corresponding author:

Tel: +55-65-992496255. E-mail robsonssouto@gmail.com (Robson Souto)

Tel: +55-16-999750504. E-mail marcoslanza@usp.br (Marcos Lanza)

Keywords

Electrochemical Flow Reactor; H_2O_2 Electrogeneration; Gas Diffusion Electrode; Response Surface Methodology; Design of Experiment; Residence Time Distribution; Single-Pass System;

ABSTRACT

This study focuses on a electrochemical flow reactor (EFR) utilizing a gas diffusion electrode (GDE) for in situ hydrogen peroxide production via the oxygen reduction reaction. Existing literature lacks comprehensive investigations into GDE-based EFR hydrodynamics and their correlation with electrochemical effects. To address this, the researchers employed response surface methodology (RSM) to analyze the hydrodynamic behavior of the GDE-based EFR. The study used flow rate and inter-electrode gap as RSM variables to analyze hydrodynamics. Residence time distribution (RTD) was employed to assess hydraulic effects and compare with H_2O_2 kinetics, revealing insights into hydraulic and electrochemical influences. Findings highlighted the importance of hydrodynamic residence time in the EFR and its impact on H_2O_2 production. RSM analysis evaluated electrochemical conditions (energy consumption, applied current, and oxygen efficiency) using variables such as current density, O_2 flow rate, and conductivity. The resulting regression equation accurately predicted in situ H_2O_2 production cost, aligning well with experimental results. The study compared a single-pass system to a common recirculating system in EFRs, revealing a 32.4% increase in H_2O_2 electrogeneration efficiency in the former. In summary, this study provides valuable insights into GDE-based EFR hydrodynamics through RSM-based modulation of operational conditions. These findings facilitate EFR technology scaling and improve H_2O_2 production efficiency.

1 Introduction

Hydrogen peroxide (H_2O_2) is a well known environmentally friendly oxidizing agent which is commonly applied in a wide range of areas, including waste water treatment and pollutant degradation, as precursor of hydroxyl radical [1]. Apart from that, the outbreak of the COVID-19 pandemic has also fuelled an increasingly growing interest among researchers regarding the use of hydrogen peroxide as an important sanitizer [2,3]. Currently, the anthraquinone oxidation (AO) method is the technique widely applied for the industrial-scale production of H_2O_2; this method involves the use of high amount of energy and harmful waste products, as well as high storage and transport costs [4]. The AO method is not environmentally friendly, since the organic solvent used in the process releases hazardous waste which poses serious risks to human and animal health, as well as to the environment. Another method used for the production of H_2O_2 involves the application of H_2 and O_2 for radicals generation and recombination in a clean water system; the problem with this technique is that it is extremely less efficient when applied toward the production of H_2O_2 [5]. In this context, the use of oxygen reduction reaction (ORR) can help overcome the main underlying constraints exhibited by the AO method through the use of O_2, including atmospheric O_2, for the *in situ* production of H_2O_2 [6].

The electrochemical flow rector (EFR) is an essentially important technology which can be easily employed in scale-up applications including wastewater treatment [7], electro-dialysis [8], energy storage processes [9], and electrosynthesis [10]. The EFR technology comes in a wide range of designs; these include parallel plate geometry, tubular, filter-press format, PEM, among other designs [11], which can be more or less suitable/desirable for the purposes intended, and this makes the EFR technique extremely adaptable. In an electrochemical flow reactor, the cathode plays an essential role in ORR, and carbon materials are the most widely used electrode material for these purposes; this is largely because carbon materials are

relatively less costly and have large active surface area, as well as good thermal and chemical stability[12]. The setup of the EFR and the electrode can mainly be done via two different liquid-flow mechanisms, namely, the flow-through system and the flow-by system; under the flow-through system, the liquid passes through/inside the electrode [13], while in the flow-by system, the system operates under a triple phase interface (gas/electrode/liquid). Among the wide range of electrode systems (planar, porous, gas diffusion electrode, etc.), the gas diffusion electrode (GDE) has attracted much attention among researchers due to its many advantages [10,14].

The use of gas diffusion electrode (GDE) helps to overcome the problem related to mass transport, as O_2 gas passes directly through the electrode in a triple phase interface (gas/electrode/electrolyte), making this electrode structure highly suitable for scale-up applications [15]. As previously pointed out by our research group in different works, the GDE system exhibits a certain degree of hydrophobicity, which facilitates the implementation of the triple phase interface; this balance has been found to be extremely important [16–18]. Taking the above considerations into account, in this present work, we report the development and application of a new electrochemical flow reactor with GDE configuration; this system, whose operating conditions, including hydrodynamic regime, mass transport, and current distribution, can be compared to a parallel plate model with liquid-phase flow-by system [19]. Although the EFR system proposed in this work has been extensively studied in the literature, there seems to be a lack of comprehensive understanding regarding the effects of the operating conditions on the EFR system. For instance, the hydrodynamic and electrochemical conditions are often treated as a single entity, even though they may have distinct impacts on the reactor performance.

For illustration purposes, Reis et al. employed GDE in an electrochemical flow-by reactor under a recirculating system to evaluate hydrodynamic and electrochemical effects

in the *in situ* electrogeneration of H_2O_2. The authors showed that, under laminar flow conditions (flow rate of 50 L h^{-1}), a maximum concentration of 414 mg L^{-1} hydrogen peroxide was generated after 2 h of electrolysis, with energy consumption of 22.1 $kWhkg^{-1}$; however, under turbulent flow (300 L h^{-1}), the flow-by system generated a maximum concentration of 294 mg L^{-1} hydrogen peroxide after 2 h of operation, with energy consumption of 30.1 $kWhkg^{-1}$[20]. Interestingly, other studies reported in the literature have also noted a similar behavior though they did not further evaluate the hydrodynamic effects [21]. Thus, it is essentially important to thoroughly evaluate these two conditions – laminar flow and turbulent flow, individually in order to gain a more comprehensive understanding of their effects on the performance of the reactor.

The residence time distribution (RTD) mechanism is an interesting approach for characterizing and determining the hydrodynamic behavior in certain flow rate operational conditions. The RTD mechanism helps determine the hydrodynamic characteristics of the reactor through macromixing information, and this can be used to make a diagnosis regarding the regime of the flow pattern of non-ideal reactors [22]; in essence, the information obtained from the RTD analysis is found to be extremely useful as it can be correlated with hydrogen peroxide generation in the EFR reactor. To the best of our knowledge, there is a scarcity of studies in the literature regarding the characterization of RTD in GDE-based EFRs [23–25]. Thus, the present study seeks to shed light on these issues that are still unclear in the area.

In this present work, we report the development and application of a new modular electrochemical flow reactor with GDE configuration applied for the *in situ* production of H_2O_2. The RTD method was used to characterize the hydrodynamic behavior of the EFR, and the data obtained were used for the conduct of a comparative analysis using the H_2O_2 electrogeneration kinetics. In addition, a macroscopic model was employed as a practical

tool for obtaining a better description of the flow regime inside the reactor; this model shows the impact of the hydraulic pattern on EFR in terms of H_2O_2 production – a relevant issue which has not yet been explored in the literature. The variables, namely, current density, gas flow, and conductivity were used for matrix construction in a design of experiments; the response surface methodology (RSM) technique was used to evaluate the parameters, namely, energy consumption ($kWhkg^{-1}$), current efficiency (%), and H_2O_2 generation (mg L^{-1}). To the best of our knowledge, the approach adopted here has not yet been explored in the literature when it comes to the analysis of GDE-based EFRs. The results obtained in this study show that the flow system can be modulated for on-demand H_2O_2 generation in real applications. Finally, a comparative analysis was conducted in order to compare the efficiency of a single-pass system with that of a recirculating system in the proposed EFR. In short, this work aims to present a novel approach for the analysis of hydrodynamic behavior in GDE-based EFRs, where RSM is also used for modeling the system in real cases for scale-up application purposes.

2 Materials and Methods

2.1 Chemicals

For the preparation of the electrolyte and pH control, the following compounds were used: sulfate potassium (K_2SO_4), sulfuric acid (H_2SO_4), potassium hydroxide (KOH). Nitric acid (HNO_3) and H_2SO_4 were used for the removal of metals from carbon matrix. The RTD test was performed using chloride potassium (KCl). For the determination of hydrogen peroxide, a complex was prepared using 0.5 mol L^{-1} H_2SO_4 solution containing ammonium molybdate ($(NH_4)_6Mo_7O_{24}$). All the compounds (acquired from Vetec) employed in the experiments were of high purity grade. Ultrapure water obtained from a Milli-Q system (resistivity >18 MΩ cm) was used to prepare all the solutions.

2.2 Preparation of Gas Diffusion Electrode (GDE)

For the synthesis of the electrode, commercial carbon powder Printex L6 carbon – PL6C, purchased from Evonik, was used as diffusion layer on the surface of a carbon fabric, acquired from ZOLTE. Poly(tetrafluoroethylene) (PTFE), (60% aqueous dispersion), obtained from daklon 1 (sealflon), was used to produce a disperse and homogeneous carbon mass and to endow the carbon electrode with hydrophobicity. In order to remove any inactive metal from the commercial carbon matrix, an acidic solution composed of 0.5 M HNO_3/H_2SO_4 was used for leaching. For the preparation procedure, the following steps were implemented: 0.6g of PL6C was added to 500 mL of acidic solution placed in a beaker, and the mixture was sonicated for 10 min. Subsequently, the PL6C-containing mixture was subjected to magnetic stirring for 8 h at 50°C. In the next step, diffusion catalytic mass was prepared by mixing the PL6C acid with 20% of PTFE (w/w) in ultrapure water and the mixture was stirred constantly for 1 h. After that, the mass was filtered and spread in a thin layer over a carbon fabric, with geometric surface area of 20 cm^2, and heated at 110 °C for 10 min (to remove excess of water). Finally, the mixture was hot-pressed through the application of 4.5 ton at 290 °C for 15 min – this procedure was adapted from the work of Cordeiro-Junior et al. [26].

2.3 Electrochemical flow reactor

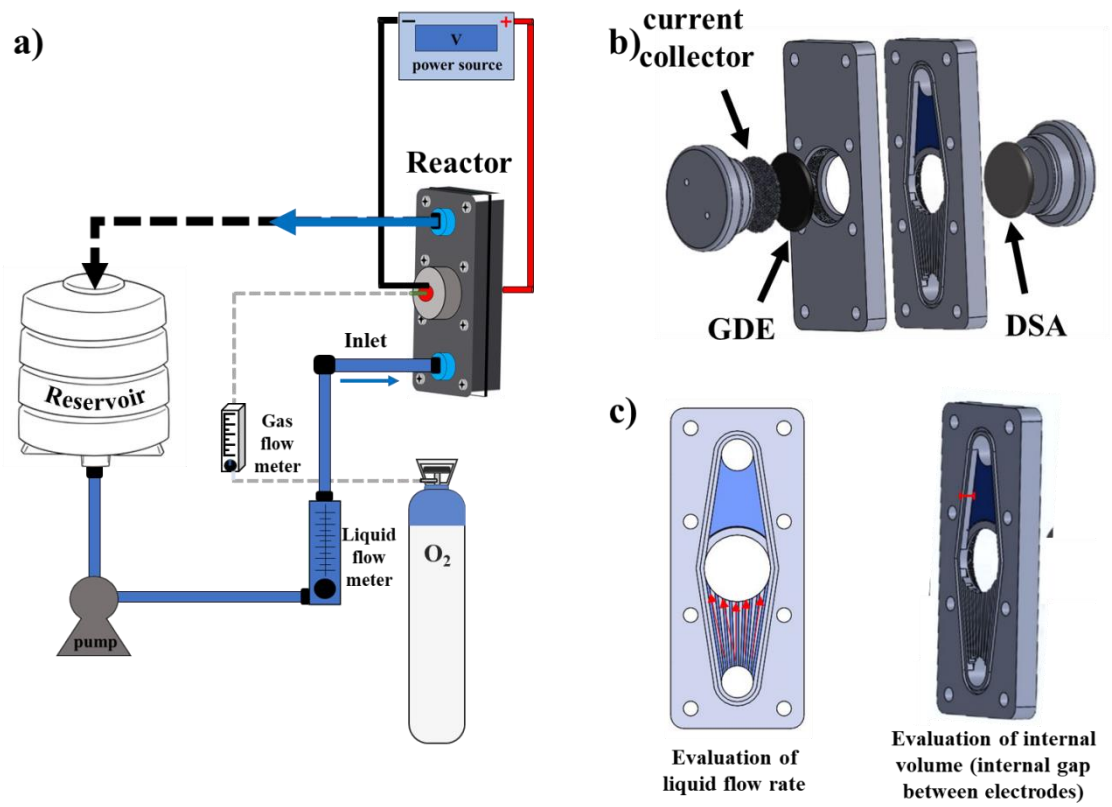

Fig. 1. **a)** Electrochemical flow reactor setup (blue arrow represents the single-pass system and the black dashed arrow represents the recirculating system); **b)** scheme illustrating the reactor setup, with the DSA anode, cathode gas diffusion electrode (GDE), and current collector; **c)** reactor internal design.

Fig. 1a presents the configuration of an electrochemical flow reactor. For the single-pass system, the electrolyte placed in the reservoir passes through the hydraulic pump-flow meter, which controls the flow rate, before going into the electrochemical reactor and moving out. In the recirculating system, the output is connected to the reservoir, which closes the loop. The oxygen cylinder provides the gas pressure, controlled by a manometer, to a flow meter which controls the gas flow into the gas diffusion electrode. The current density is controlled by a power supply, which is connected to the electrochemical reactor. For the anode electrode, we employed a dimensionally stable anode-chloro alkali (DSA-Cl_2, with exposed area of 20 cm^2, from De Nora do Brasil), with the same geometric area as the cathode. The scheme illustrating the reactor design is shown in Fig. 2b, with the mechanism

involving the assembly of the system. The two plates have internal designs, which are demonstrated in Fig. 1c, with different depths that allow one to vary the volume of the internal system.

The quantification of the amount of hydrogen peroxide electrogenerated was performed using UV-1900 spectrophotometer (Shimadzu) with 0.2 mL H_2O_2 and 4.3 mL $(NH_4)_6Mo_7O_{24}$ solution (2.4×10^{-3} mol L^{-1}). The complex formed, with molybdate and H_2O_2 (peroxymolybdate), is very stable, with absorbance at 350 nm wavelength[27]. The parameters, namely, current efficiency (eq. 1) and energy consumption (eq. 2) were used for the analysis of the electrochemical efficiency of the reactor system.

$$\mathrm{CE}(\%) = \frac{2\,\mathrm{F}\,\mathrm{C}\,\mathrm{V}}{It_1} x\ 100 \qquad \textbf{(eq. 1)}$$

$$\mathrm{EC}(\mathrm{kWh}\ kg^{-1}) = \frac{1000\,\mathrm{E}\,\mathrm{I}\,t_2}{M} \qquad \textbf{(eq. 2)}$$

In the CE equation (eq. 1) , the value 2 represents the electron transfer for O_2 reduction, F stands for Faraday constant (96,487C mol^{-1}), C (mol L^{-1}) represents the concentration of H_2O_2, V is the volume inside the reactor, and I (A) is the current that passes through the cathode at time t_1 (s). In the EC equation (eq. 2), E (V) stands for potential, I (A) is the current that passes through the electrode at time t_2 (h), and M is the mass in kg of H_2O_2 electrogenerated.

2.4 Residence Time Distribution (RTD) Analysis

The flow pattern of the EFR was evaluated using RTD with tracer pulse methodology [28]. To conduct this analysis, 1 mL of the tracer (potassium chloride, $[KCl]_0$ = 3 mol L^{-1}) was injected with a syringe near the EFR inlet and measured at the EFR exit using a conductivity meter (Digimed). The tracer pulse experiments were performed using varying reactor internal volumes (5, 10 and 15 mL) and volumetric flow rates (15, 30 and 45 L h^{-1}). The

conductivity values obtained were then transformed into concentration (C(t)) by means of a calibration curve previously obtained and used to construct the RTD curves. All the assays were performed in triplicate.

The tracer concentration (C(t)), measured at the reactor outlet, was used to calculate the exit function, E(t), as a function of different EFR flow rates and volumes, according to the following equation [22]:

$$E(t) = \frac{C(t)}{\int_0^\infty C(t)dt} \quad \textbf{(eq. 3)}$$

The average residence time (t_m) was calculated relative to E(t), as follows:

$$t_m = \frac{\int_0^\infty tE(t)dt}{\int_0^\infty E(t)dt} = \int_0^\infty tE(t)dt \quad \textbf{(eq. 4)}$$

To evaluate the deviation from ideal behavior, the space time (τ) was calculated using the following equation [22]:

$$\tau = \frac{V}{\upsilon_0} \quad \textbf{(eq. 5)}$$

where V(mL) is reactor internal volume, and υ_0 is the flow rate (L h^{-1}).

In addition to the first moment (t_m), the variance (σ^2) and the distortion (s^3) of the distribution are other moments usually used to compare the hydrodynamic behavior for different flow conditions, as given by the following equations:

$$\sigma^2 = \int_0^\infty (t - t_m)^2 E(t)dt \quad \textbf{(eq. 6)}$$

$$s^3 = \frac{1}{\sigma^{\frac{3}{2}}} \int_0^\infty (t - t_m)^3 E(t)dt \quad \textbf{(eq. 7)}$$

In this sense, combining the RTD characterization data with the macroscopic model is a practical way of gaining a better understanding of the flow behavior inside the reactors. Among the numerous models proposed in the literature, the present work employed the

models found to be the most outstanding, which included the following [28]: 1) Laminar-flow reactor (LFR) model, which has only one parameter (t_m) and assumes a laminar flow in the reactor; 2) Tanks-in-series (T-I-S) model, which divides the entire volume into a number (N) of stirred tanks of equal capacity with t_m; 3) CSTR + PFR in series model, which describes the EFR as a continuous stirred-tank reactor (CSTR) coupled to a plug flow reactor (PFR) in series with $t_m = \tau_{CSTR} + \tau_{PFR}$; 4) Axial dispersion (AD) model, which measures material dispersion throughout the reactor using the Peclet number (Pe) and t_m.

2.5 Design of experiments (DoE)

When it comes to the analysis of the hydrodynamic behavior of electrochemical flow reactors, the Doehlert method is applied for the design of experiment, since only two variables are intended to be analyzed: the inter-electrode gap (mm) and the flow rate (Lh^{-1}). The matrix related to the two variables is presented in Table S1; it consists of nine experiments, three of them in the central point. The variables are coded using the follow equation.

$$X_i = \left(\frac{U_i - U_0}{\Delta U_i}\right)\alpha_i \qquad \textbf{(eq. 8)}$$

The term X_i is the value coded for i factor level, U_i is the real experimental value and U_0 is the central value. ΔU_i is the difference between the highest and the lowest value for U_i, and α_i is the coded value limit for each factor. The response function (Y) is a second order polynomial function expressed by the following equation:

$$Y = b_0 + b_1X_1 + b_2X_2 + b_{11}X_{11}^2 + b_{22}X_{22}^2 + b_{12}X_1X_2 \qquad \textbf{(eq. 9)}$$

where b_0, b_1 and b_2 are the model coefficients, determined by the Octave software; this can be found in Table S2.

For the analysis of the electrochemical condition of the reactor and modeling the parameters adopted, the Box-Behnken design of experiments was used; this is because the

variables oxygen flow and current density have boundary experimental range for the system employed, making this model more suitable[29]. The variables analyzed were O_2 flow ($Lmin^{-1}$), current density ($mAcm^{-2}$) and energy consumption ($kWhkg^{-1}$); the coded matrix is presented in Table S4, with 15 experiments in order. The real values are coded based on equation 8. The polynomial equation as a function of Y is expressed below:

$$Y = b_0 + b_1X_1 + b_2X_2 + b_3X_3 + b_{11}X_{11}^2 + b_{22}X_{22}^2 + b_{33}X_{33}^2 + b_{12}X_1X_2 + b_{13}X_1X_3 + b_{23}X_2X_3 \quad \textbf{(eq. 10)}$$

The coefficients (b_0, b_1, b_2, b_3 and their interactions) obtained from the Octave software, for each of the parameters adopted, including CE, H_2O_2 concentration and EC, can be found in Tables S6, S8 and S10, respectively. For both design of experiments methods, the fit polynomial model was evaluated via R^2 and its statistical significance, using the Fisher F test, with 95% confidence p-value level. The interaction between the independent variables and the responses was evaluated via the analysis of variance (ANOVA) - see Tables S3, S7, S9 and S11.

3 Results and discussion

3.1 Hydrodynamic behavior

3.1.1 Modeling hydrodynamic parameters

To gain a better understanding of the hydrodynamic behavior of the electrochemical flow reactor proposed in this study, we used the Doehlert methodology as a design of experiments to model the response surface for H_2O_2 concentration. In this set of experiments, we kept the electrochemical operating conditions constant, and we changed only two variables related to the analysis of H_2O_2 production: the liquid flow rate and the inter-electrode gap (distance between electrodes). The inter-electrode gap was adjusted by increasing or decreasing the inside height while maintaining the same flow design. It is worth pointing out that the adjustment of the inter-electrode gap also changes the reactor internal

volume; this will be discussed in detail in the next section on the characterization of the hydrodynamic behavior.

It is important to note that the variables flow rate and inter-electrode gap (the distance between the electrodes) directly influence the velocity (ν) with which the electrolyte passes through the EFR. For example, at the same distance between the electrodes, an increase in the flow rate results in a greater electrolyte velocity; similarly, at the same flow rate, an increase in the space between the electrodes will lead to a decrease in the electrolyte velocity, allowing the same volume per time (flow rate) to pass through a larger inter-electrode gap. In this sense, the velocity of passage of the electrolyte through the EFR is a parameter dependent on the flow rate and the inter-electrode gap and must be analyzed in the H_2O_2 generation process. Fig. 2 presents a response surface graph which shows H_2O_2 concentration in relation to flow rate and inter-electrode gap, and where the different reactions that occur inside the EFR are demonstrated.

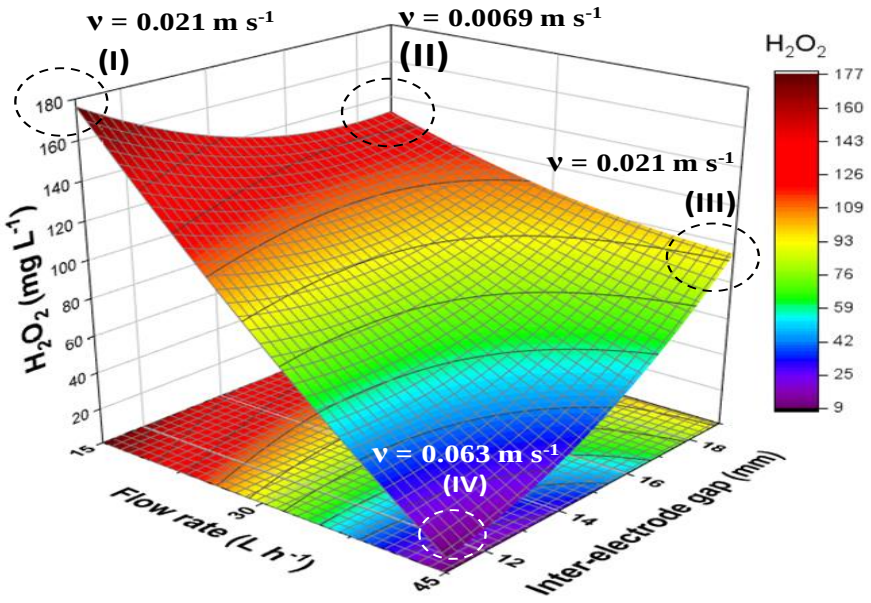

Fig. 2. Response surface of flow rate (**Q**) and inter-electrode gap (**D**) for the proposed reactor as a function of H_2O_2 concentration with the respective velocity (m s^{-1}) at each end of the response surface. Reaction conditions: current density of 150 mA cm^{-2}; 100 mL min^{-1} O_2 flow rate; and 0.05 M of K_2SO_4 employed as supporting electroyte.

The combined application of low inter-electrode gap (11 mm) and high flow rate (45 L h^{-1}), **IV**, resulted in the highest internal velocity, 0.063 m s^{-1}, with the generation of a small concentration of H_2O_2 (9.0 mg L^{-1}); this outcome may be attributed to the greater hydrodynamic force on the GDE, which causes a decrease in the electrode-gap interface due to the entry of small amounts of electrolyte into the electrode structure.

An increase in the inter-electrode gap to 19 mm (keeping the flow rate constant (at 45 L h^{-1}), **IV to III**, led to the production of a significantly higher concentration of H_2O_2 (95 mg L^{-1}); essentially, the variation in the distance between the electrodes, at the same flow rate, promoted a reduction in the electrolyte velocity (0.021 m s^{-1}), and this led to a significant increase in H_2O_2 generation (95 mg L^{-1}). The increase in H_2O_2 generation may be attributed to an equilibrium observed in the minimum velocity for the removal of bubbles from the GDE surface, but which is not sufficient for the electrolyte to penetrate into the electrode structure[30].

Based on the results obtained from our analysis, region **I,** which possessed the lowest flow rate (15 L h^{-1}) and inter-electrode gap (11 mm) exhibited relatively higher amount of H_2O_2, 176 mg L^{-1}, compared to region **III**, which had the highest flow rate (45 L h^{-1}) and inter-electrode gap (19 mm). It is worth noting that the increase observed in H_2O_2 generation may be the result of a series of changes in the experiments; these include the changes related to the ideal electrolyte velocity for the renewal of the surface of the electrodes, with the removal of bubbles, and the minimal penetration of the electrolyte into the GDE structure. Another important point that deserves being mentioned is the reduction of the inter-electrode gap, which led to the reduction of the ohmic drop in the system. These factors jointly contributed to an increase in H_2O_2 generation within the parameters investigated.

When the flow rate was kept low (15 L h^{-1}) and the inter-electrode gap was increased from 11 mm (**I**) to 19 mm (**II**), we observed a slight decrease in H_2O_2 generation (reaching 138 mg L^{-1}). An increase in the inter-electrode gap and the application of the same flow rate (15 L h^{-1}) led to a significant reduction in the internal velocity of the electrolyte (0.0069 m s^{-1}). This internal velocity of the electrolyte was found to be insufficient for the efficient removal of bubbles from the GDE surface. Thus, as previously described in other works, the application of a higher inter-electrode gap resulted in an increase in the ohmic drop and a decrease in H_2O_2 generation [31,32].

The response surface methodology (RSM) is an effective tool for evaluating a wide range of operational conditions of the flow reactor system; regarding the electrochemical flow reactor investigated in this study, we were able to clearly observe the effect of the flow rate and the inter-electrode gap on the production of H_2O_2 in the EFR. Thus, the RSM applied in this work provides us with a very accurate prediction regarding the concentration of H_2O_2 under the conditions investigated through a polynomial equation. Equation 11 below shows the polynomial equation for the prediction of H_2O_2 concentration under varying conditions of flow rate and inter-electrode gap (in the electrochemical reactor):

$$[H_2O_2] = 81.4 + (10.4 * D) + (-58.9 * Q) + (14.9 * D^2) + (8.8 * Q^2) + \big(37.8 * (D * Q)\big) \quad \textbf{(eq. 11)}$$

The RSM (see Fig. 2) clearly demonstrates that the flow rate and inter-electrode gap exert significant effects on the amount of hydrogen peroxide concentration produced in the system, and one can use a model equation to predict the amount of H_2O_2 with the variation of these variables (flow rate and inter-electrode gap). An in-depth discussion on this topic will be provided in the next sections when we compare the hydrodynamic behavior with the kinetic effects.

3.1.2 RTD evaluation

The residence time distribution (RTD) is a powerful tool for evaluating the hydrodynamic behavior inside electrochemical flow reactors (EFR); this is because through the application of this analytical tool, one can alter the liquid flow rate and the internal volume, and this may lead to changes in the flow pattern of the EFR. Bearing that in mind, we conducted three experiments with the same EFR setup using 5 mL internal volume with variation in the liquid flow rate (from 15 to 45 L h^{-1}). Another experiment was also conducted where the liquid flow rate was kept at 30 L h^{-1} while the internal volume was changed from 5 to 15 mL. In both the aforementioned experiments conducted, the main goal was to analyze the E(t) (eq. 3), which represents the function of residence time distribution; the RTD provides us with a quantitative description regarding the amount of time the fluid element spent in the EFR. The mean residence time (t_m) represents the average time spent by the fluid element inside the EFR - the E(t) equation is used for the conduct of these calculations. Another important parameter is the space time (τ), which represents the time required to feed the internal reactor volume. Furthermore, the dimensionality of variance (σ^2) and distortion (s^3) is a very important parameter that shows how far the RTD is from the ideal flow pattern. Fig. 3 shows typical experimental RTD curves obtained for the EFR. A thorough discussion on these curves can be found below.

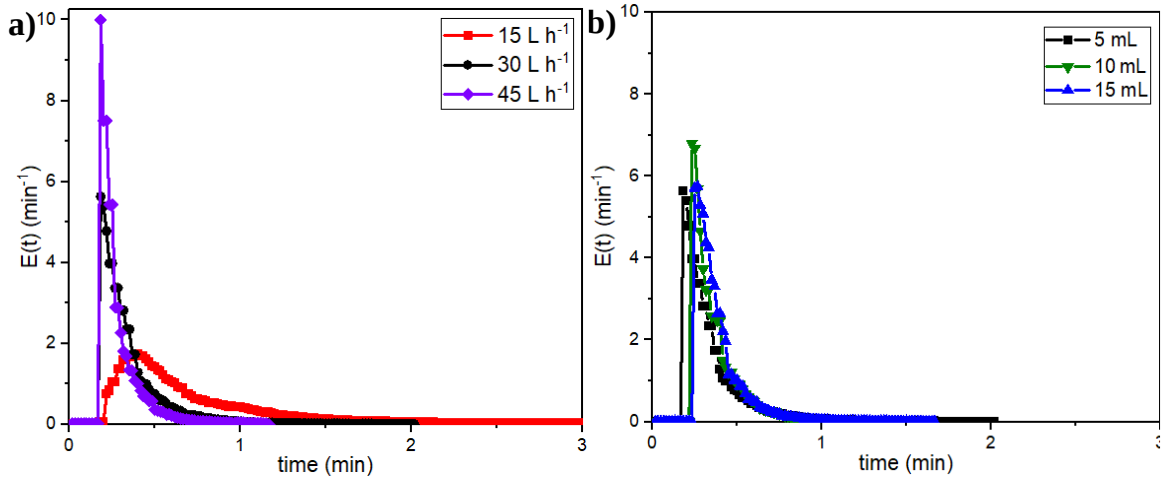

Fig. 3. RTD curves for **a)** different flow rates in the reactor with 5 mL internal volume, and **b)** different reactor volumes operating at 30 L h^{-1}.

Using a fixed reactor volume (5 mL) (Fig. 3a), one notices that as the volumetric flow rate increases, the fluid elements are forced out of the reactor more quickly with t_m varying between 0.29 and 0.74 min (as can be seen in Table 1). In addition, an interesting correlation is observed between the flow rate and the variance (σ^2) and distortion (s^3) (Table 1); this correlation points to a greater deviation from the mean values and the increase observed in the amount of the fluid elements points to a flow delay, linked to the long tail of the curves. The shear stress on the reactor walls is responsible for the low velocity zones that are indicated by such a tail in the RTD curves and is associated with possible stagnant regions inside the reactor geometry, short-circuiting, by-passing, and fluid channelling [19]. When the flow rate is kept constant at 30 L h^{-1} and the reactor internal volume is changed, one observes that the experimental curves become remarkably close (Fig. 3b); this is corroborated by the similar t_m (varying between 0.36 and 0.39 min) and the low variations observed between the other calculated moments (σ^2 and S^3) (Table 1). Finally, the RTD results obtained are found to be in good agreement with the experimental data on the amount of H_2O_2 generated (Fig. 2); in essence, this shows that higher fluid residence times in the EFR are responsible for greater H_2O_2 generation, which can be controlled by

varying the flow rate and the EFR volume, with the flow rate exerting an even more significant effect (eq. 11).

Table 1. Values obtained for the parameters evaluated in the RTD experiments.

V(L)	Q (L h^{-1})	τ(min)	t_m (min)	σ^2 (min^2)	s^3 (min^3)
$5.0x10^{-3}$	15	$5.3x10^{-2}$	0.74	0.28	0.81
$5.0x10^{-3}$	30	$2.6x10^{-2}$	0.36	0.05	0.33
$5.0x10^{-3}$	45	$1.8x10^{-2}$	0.29	0.02	0.13
$1.0x10^{-2}$	30	$3.6x10^{-2}$	0.37	0.03	0.16
$1.5x10^{-2}$	30	$4.6x10^{-2}$	0.39	0.03	0.20

Under the macroscopic analytical approach, the RTD data (e.g. mean residence time (t_m), Peclet number (*Pe*)) are used to simulate the flow regime of non-ideal reactors. This macroscopic characterization can be performed based on the deviations (the variance (σ^2) and the distortion (s^3)) obtained from the RTD analysis, and may oscillate between two main ideal flow reactor models: plug-flow reactor (PFR) or continuous stirred-tank reactor (CSTR) - which is based on a perfectly mixed pattern [18]. These two ideal models have opposite responses: the PFR exhibits complete radial mixing in the longitudinal direction and it is characterized by constant velocity profiles over the flow length. On the order hand, the CSTR shows an exponentially decaying RTD profile, such that the fluid in the reactor outlet stream will always have an identical composition. In non-ideal reactors, the deviations present in the hydrodynamic behavior can be caused by non-uniform velocity, due to turbulent diffusion, stagnant regions inside of the reactor geometry, short-circuiting, by-passing, and fluid channelling [19]. Other models can be proposed based on the calculated deviation in the RTD analysis; these models include the Laminar-flow reactor (LFR) model, the Tanks-in-series (T-I-S) model, and the Axial dispersion (AD) model. The macroscopic flow in the electrochemical flow reactor was evaluated using the LFR, T-I-S, CSTR + PFR, and AD models, as shown in Fig. 4.

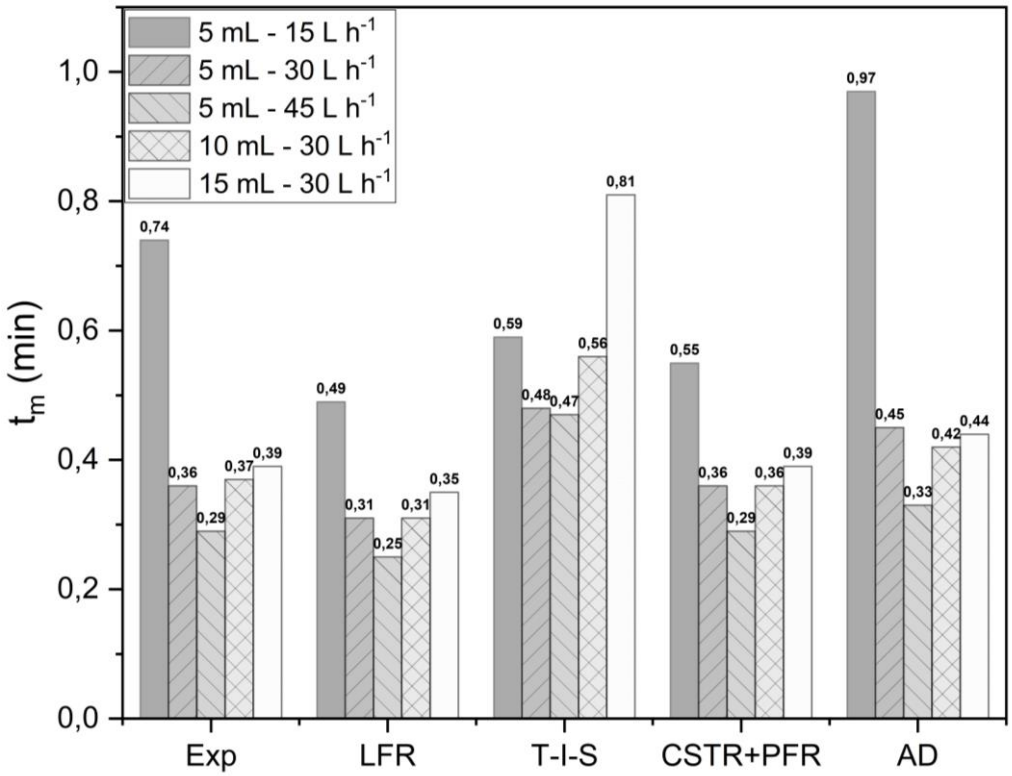

Fig. 4. A comparative analysis of the macroscopic approaches and experimental data for the description of the flow pattern in the EFR based on the residence time distribution.

In Fig. 4, the experimental (Exp) data show the parameters that can be compared with the other proposed models. The LFR model was unable to explain mixing patterns, as this model projected t_m lower than the experimental values. In this regard, the T-I-S model which represented the EFR between 2 to 6 of CSTRs in series of equal size, and the AD model with *Pe* between 7-15 failed to explain the non-ideality of the EFR, since the values obtained for t_m were greater than the experimental values under the different conditions investigated. Interestingly, the CSTR + PFR model was able to better represent the asymmetries of the curves and the respective non-idealities with accurate t_m values in relation to the experimental data (Fig. 4). The asymmetries of the curves can be well explained (Fig. 3) by the contribution of the CSTR relative to the intense fluid mixing observed at the reactor entrance, followed by the contribution of the PFR, which indicated a better flow distribution, attributed to the presence of the flow distributor placed after the EFR inlet (Fig. 1). This makes the

CSTR + PFR model the most suitable macroscopic model for explaining the fluid flow in the EFR. Comparable results were observed for a reactor with annular geometry which pointed to a contribution of the CSTR, stemming from the inlet port, and PFR contribution, attributed to the helical (spiral) fluid flow with the validation of the CFD model [33].

3.1.3 The Influence of Flow Pattern on H_2O_2 electrogeneration

To validate the proposed model using RSM (Fig. 2) and correlate the flow patterns obtained through RTD analysis, we conducted a kinetics study of H_2O_2 concentration over time at the same flow rates observed in Fig. 3.

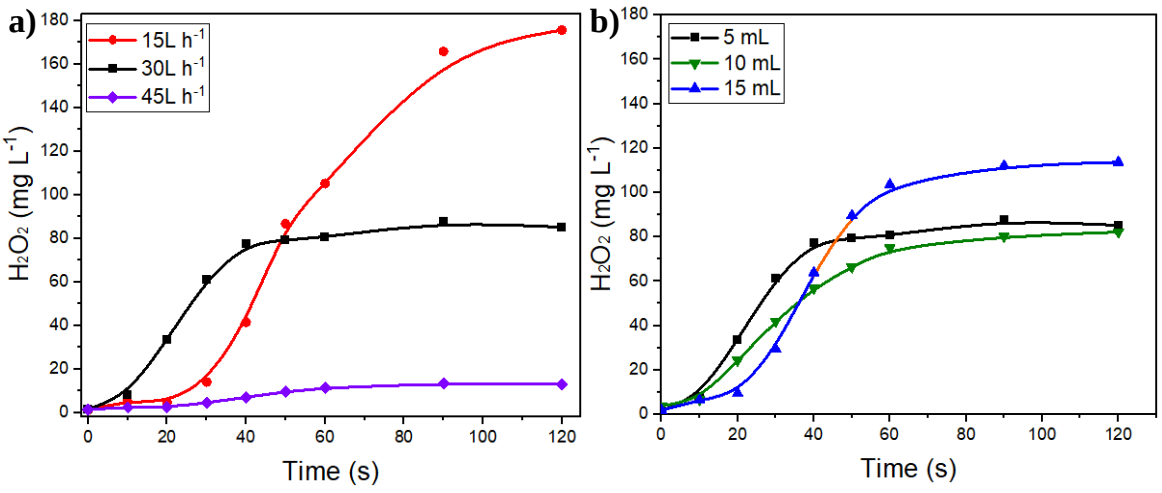

Fig. 5. Analysis of H_2O_2 electrogeneration through the application of **a)** 5 mL reactor internal volume at different flow rates, and **b)** 30 L h^{-1} flow rate at different reactor internal volumes.

The EFR was analyzed based on the application of 5 mL of internal volume at the flow rates of 15, 30, and 45 L h^{-1} (Fig. 5a). As expected, at a higher flow rate (30 L h^{-1}), the curve increases at ~10 seconds, but when the flow rate is reduced (15 Lh^{-1}), the concentration begins to rise after 20 seconds; these outcomes are in agreement with the RTD behavioral patterns (see Fig.3a). It should be noted however that the amount of H_2O_2 generated at a higher flow rate (81 mgL^{-1}) is half the amount recorded at a lower flow rate (181 mgL^{-1}); this outcome can be explained by the hydrodynamic residence time (0.35 and 0.72 min, respectively). It is worth noting that the amount of H_2O_2 generated is found to be in line with

the confidence interval of the proposed regression equation (176 and 85 mgL^{-1} at 15 and 30 Lh^{-1}, respectively).

Fig. 5b shows the results obtained from a comparative analysis conducted using different reactor internal volumes (5, 10 and 15 mL) at the same flow rate (30 L h^{-1}). As predicted by the RTD analysis (Fig. 3-b), the increase observed in H_2O_2 concentration was almost the same for each reactor internal volume; however, the amount of H_2O_2 concentration generated can be clearly distinguished. For the application of 15 mL reactor internal volume, the amount of H_2O_2 generated was 113 mg L^{-1}, while the application of the internal volumes of 5 and 10 mL yielded almost the same amount of H_2O_2 concentration (86 and 81 mgL^{-1}, respectively). The similar amount of H_2O_2 concentration obtained for the internal volumes of 5 and 10 mL can be explained by the hydrodynamic residence (0.35 min for both). At the internal volume of 15 mL, one notices a slight increase in residence time (0.36 min), which contributes toward an increase in H_2O_2 concentration by approximately 31%; this behavior is also predicted by the RSM, as shown in Fig. 2 for the yellow range on the graph, which displays the amount of H_2O_2 obtained from the application of a 30 Lh^{-1} flow rate at different internal volumes. It is worth emphasizing that the H_2O_2 concentration in all configurations was found to reach its maximum value after two minutes of flow and remained stable with slight fluctuations at a plateau – see Fig. S1 which shows H_2O_2 electrogeneration in 30 minutes of electrolysis. This behavior may be attributed to the bubbles introduced by the gas diffusion electrode (GDE) configuration, which has been previously observed in other works[34].

Remarkably, the hydrodynamic behavior observed in our present study is not a new phenomenon in the literature. Oloman and Watkinson (1979) employed a trickle bed electrochemical reactor, with graphite particle as cathode, for hydrogen peroxide production. According to the authors, an increase in the cathode bed length (from 2 to 4 m) with no

changes to the flow rate resulted in an increase in H_2O_2 concentration. Conversely, an increase in the flow rate (from $2.1x10^{-5}$ to $3.1x10^{-5}$ L h^{-1}) led to a reduction in the amount of hydrogen peroxide generated [35]. In a recent study reported by Li et al., the authors employed an electrochemical cell with carbon black-polytetrafluoroethylene GDE for H_2O_2 production where they evaluated the techno-economic feasibility of the technique when applied in decentralized water treatment systems. The authors successfully demonstrated the correlation between hydraulic residence time (HRT) and hydrogen peroxide concentration, where the application of flow rate ranging between 40 to 5 mL min^{-1} resulted in an increase in HRT from 10 to 80 min and an increase in the amount of H_2O_2 generated from 94 to 349 mgL^{-1}[36].

Curiously, theses previous studies have often considered the hydrodynamic and electrochemical effects as a single entity when studying H_2O_2 production in electrochemical flow reactors[24,25,31]. To truly understand the role of hydrodynamic effects on electrochemical reactor design and the gas diffusion electrode (GDE) in H_2O_2 production, it is essentially important to separate these two effects. To the best of our knowledge, previous studies reported in the literature focused their analyses on the relationship between flow rate and H_2O_2 electrogeneration without exploring the existing correlation between these elements and the hydrodynamic behavior separately. Thus, this study provides two pieces of information that can help explain the general hydrodynamic behavior observed in the electrochemical reactors: i) the relationship between the residence time in the reactor and H_2O_2 accumulation, and ii) the effect of the GDE configuration on the stability of H_2O_2 concentration over time. The analytical approach proposed in this study allows for better control of the amount of H_2O_2 accumulation by adjusting the flow rate, and a regression equation can be used to model the system. Overall, separating the hydrodynamic and

electrode effects in this study provides valuable insights for the optimization of H_2O_2 concentration in electrochemical flow reactors based on GDE systems.

3.2 Design of Experiments (DoE) Applied to Electrochemical Models

3.2.1 Current Efficiency and Oxygen Flow Rate in H_2O_2 Electrogeneration

Current efficiency (CE) is a key parameter that indicates the amount of electric charge that passes through the electrode and which can be converted into H_2O_2. In this sense, CE is an important parameter for analyzing electrochemical flow reactor, considering that an increase in current density or oxygen flow leads to a higher production of H_2O_2, though it also contributes to a decrease in the efficiency of the reactor, as reported in other studies[37,38]. Thus, the analysis of CE can help us identify optimal conditions for maximizing H_2O_2 production while maintaining the high efficiency of the electrochemical reactor. As aforementioned, the gas diffusion electrode (GDE) is an outstanding electrode with several advantages; its application in electrochemical reaction helps overcome the problem related to mass transport [36]. The mass transport in GDEs can be influenced by several factors, including the thickness of the diffusion layer, the gas flow rate, and the degree of hydrophobicity. In this sense, to better evaluate the efficiency of oxygen in H_2O_2 production, O_2 gas with high degree of purity (99%) was used to analyze the efficiency of GDE in terms of H_2O_2 production. Fig. 6 shows the response surface graphs for the variables current density and oxygen flow in relation to current efficiency (CE) and hydrogen peroxide concentration (H_2O_2), respectively.

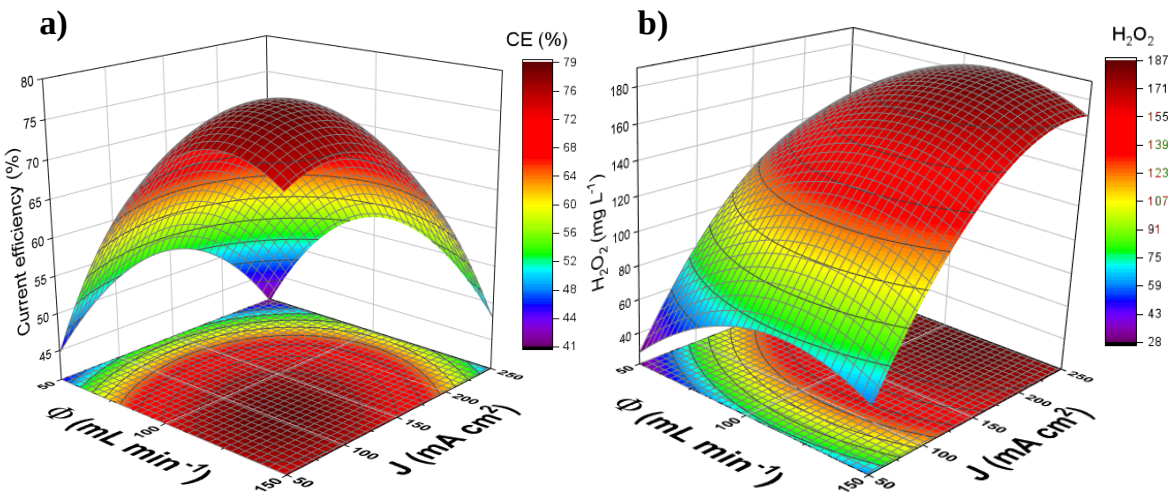

Fig. 6. Response surface of the variables current density (**J**), O_2 flow rate (**Φ**); **a) Φ** vs **J** relative to current efficiency (CE); **b) Φ** vs **J** relative to hydrogen peroxide concentration (H_2O_2).

As shown in Fig. 6a, the maximum CE is represented by the white region on the graph and indicates an efficiency of approximately 78.4% under moderate conditions (125 mA cm^{-2} and 100 mL min^{-1} of O_2 flow). Both oxygen flow rate and current density have a direct influence on H_2O_2 electrogeneration and can be considered as reactants in the reaction, as described in Eq. 12 below.

$$O_2 + 2H^+ + 2e^- \rightarrow H_2O_2 \qquad \textbf{(eq. 12)}$$

Taking the above considerations into account, the gas diffusion electrode (GDE) is thus a crucial component of the electrochemical reactor setup which has a significant impact on the CE of the reactor. The composition and configuration of the GDE can enhance the conversion of current and oxygen into H_2O_2. Several studies have shown that, through the modification of the carbon matrix, one can improve selectivity for two-electron transfers from O_2 to hydrogen peroxide [39,40]. For instance, Lu et al. used tert-butyl-anthraquinone to modify various carbon materials (including carbon aerogel, carbon nanotube (CNT), carbon black, and graphene-doped carbon black) in a GDE cathode; in all the cases they

494 investigated, the modification of carbon material led to an increase in CE compared to the
495 unmodified carbon material, with the maximum CE reaching up to 95% [33].

496 Fig. 6b shows the response surface of H_2O_2 concentration when 99.9% pure oxygen
497 passes through the GDE during electrosynthesis. The highest point in the graph, which points
498 to the production of H_2O_2 concentration of 187 mg L^{-1}, can be found close to the higher O_2
499 flow rate (150 mL min^{-1}) and high current density (250 $mAcm^2$). This outcome can be
500 explained by taking into account eq. 12 and the structure of the GDE, where both O_2 and
501 electron are present in abundance near the active sites of the GDE catalytic layer. Under
502 these conditions, both the mass transport (amount of O_2 injected into the GDE structure) and
503 the excessive current load (high applied current density) favor the electrochemical
504 production of H_2O_2.

505 Carbon material electrodes offer several advantages, and this includes a higher
506 surface area which provides more active sites for the oxygen reduction reaction process to
507 occur. The presence of higher surface area leads to improved efficiency in the adsorption of
508 O_2 and its conversion into H_2O_2, as already reported in the literature [34,41]. Taking all the
509 above considerations into account, it is clear that GDE plays a crucial role in the
510 electrochemical reactor, and must be carefully considered during scale-up applications. It
511 should be noted however that the practical application of GDEs requires addressing other
512 important issues such as cost-effectiveness, energy consumption, and long-term stability.
513 Thus, research on GDEs must strive to balance performance, cost, and durability in order to
514 achieve optimal results in practical applications.

515 ### 3.2.2 Energy Consumption in H_2O_2 Electrogeneration

516 Energy consumption (EC) is also another important parameter to consider when it
517 comes to real applications of reactors; this is because EC is directly linked to the energy cost

involved in the electrosynthesis of hydrogen peroxide. In an electrochemical reactor, a wide range of variables can affect the EC; these variables may include electrode distance and liquid phase conductivity. Apart from that, in a GDE system, the bubbles formed due to excess of gas passage or oxygen deficiency can increase the resistance of the circuit. Another factor that is worth mentioning is electrode resistivity (e.g. the use of PTFE for hydrophobicity in carbon materials); this can also increase the potential and consequently the amount of energy consumed during the reaction process. It is worth pointing out that in the present work, we only considered the effect of conductivity, which is controlled by the salt (K_2SO_4) concentration, since all the other conditions were kept constant. Fig. 7 shows the response surface of i) conductivity with current density (Fig. 7a) and ii) conductivity with O_2 flow (Fig. 7b), where both relationships were evaluated in terms of energy consumption.

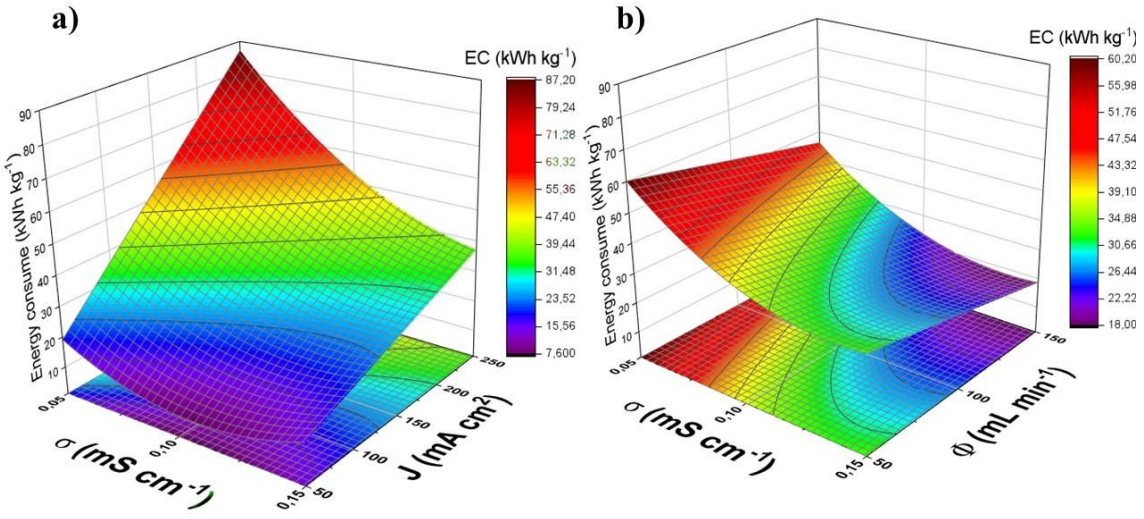

Fig. 7. Response surface of the variables current density (**J**), O_2 flow (**Φ**) and conductivity (**σ**); **a) σ** vs **J** in terms of energy consumption (EC); and **b) σ** vs **Φ** in terms of energy consumption (EC).

At low current density and higher conductivity, EC was found to be less than 10 $kWhkg^{-1}$ of H_2O_2 (Fig. 7-a). Although these relationships have been investigated in several works reported in the literature, these studies sought to evaluate the interaction involving one of these two variables with energy consum[13,42] without assessing the interaction between

the two variables, which is, in essence, one of the main contributions of the present study. Fig. 7b shows that a relatively lower EC (20 $kWhkg^{-1}$) was obtained at higher conductivity and O_2 flow; this outcome can be explained by the surface activity on the GDE which is aimed at adsorbing oxygen and converting it into hydrogen peroxide. In both the cases analyzed, the amount of energy consumed was found to be lower at higher conductivity, as expected, once the excess of ion species decreases the ohmic drop in the EFR.

As demonstrated here, conductivity exerts a significant effect on EC in the electrochemical flow reactor. In this setup, the amount of energy consumed can be controlled by the conductivity in the electrolyte, reducing the cost of H_2O_2 electrogeneration. Furthermore, wastewater effluent in general has high conductivity due to the presence of salts from different sources [43]; this reflects the need for little or no adjustment in order to maintain a reasonable degree of conductivity in the liquid phase with a view to operating an EFR in a treatment plant.

3.2.3 Proposed Equations from Response Surface Models

The response surface model, obtained through the design of experiments presented in this work, provides a mathematical equation for all variables, including current density (J), O_2 flow rate (Φ), and conductivity (σ), as a function of the adopted parameters (energy consumption (EC), H_2O_2 concentration ($[H_2O_2]$), and current efficiency (CE)). The proposed equations related to the response surface model can be found below.

$$CE = 75.7 + (-7.3 * J) + (8.9 * \Phi) + (-10.8 * J^2) + (-13.2 * \Phi^2) + \left(-5.3 * (J * \Phi)\right) \quad \textbf{(eq. 13)}$$

$$[H_2O_2] = 160.1 + (56.3 * J) + (15.3 * \Phi) + (-33.3 * J^2) + (-27.5 * \Phi^2) \quad \textbf{(eq. 14)}$$

$$EC = 30.5 + (22.6 * J) + (-7.1 * \Phi) + (-13.6 * \sigma) + (-13.6 * \sigma^2) + \left(-11.2 * (J * \sigma)\right)$$

(**eq. 15**)

The coefficients of the equations 14, 15 and 16 are presented in Tables S6, S8 and S10, respectively. It is worth noting that the coefficient values presented for all the equations were recalculated from each model, after excluding non-significant coefficients. Based on the results obtained, we were able to predict the parameter response for any variable condition applied within the range of the model. As discussed above, each parameter is directly correlated with the following elements: EFR, electrode, volume, and flow rate. The adoption of this analytical approach allows for a better evaluation of the cost and efficiency involving the production of a certain amount of hydrogen peroxide. Clearly, this is a powerful tool for industrial applications, as it enables us to modulate the variables for different situations and demands, as well as the expenditure involving the application of the process.

3.3 Single-Pass and Recirculating Systems

Most studies reported in the literature related to the design of electrochemical reactors employ a recirculating system where the electrolyte passes through the reactor and returns to the reservoir, as shown in Fig. 1. This system allows for the production and accumulation of H_2O_2 in a fixed volume. However, in this kind of system, the hydrogen peroxide is subject to decomposition through various processes, including self-decomposition and electrochemical oxidation at the anode when there is no separation between electrodes, as well as by oxidant predator species that depend on the ions in the solution [34]. The use of a single-pass system in electrochemical reactors can help overcome the aforementioned constraints by reducing the effect of the decomposition of hydrogen peroxide. In the single-pass system, the electrolyte passes only once in the electrochemical flow reactor and this helps to minimize the decomposition by anode or self-decomposition by accumulated concentration. In the present study, we performed a comparative analysis of

a single-pass system and a recirculating system, with both systems operating in the same electrochemical reactor; this analysis was conducted in order to evaluate and compare the efficiency of the systems in terms of H_2O_2 electrogeneration when operated under identical hydrodynamic and electrochemical conditions. Fig. 8 shows the results obtained from this comparative analysis.

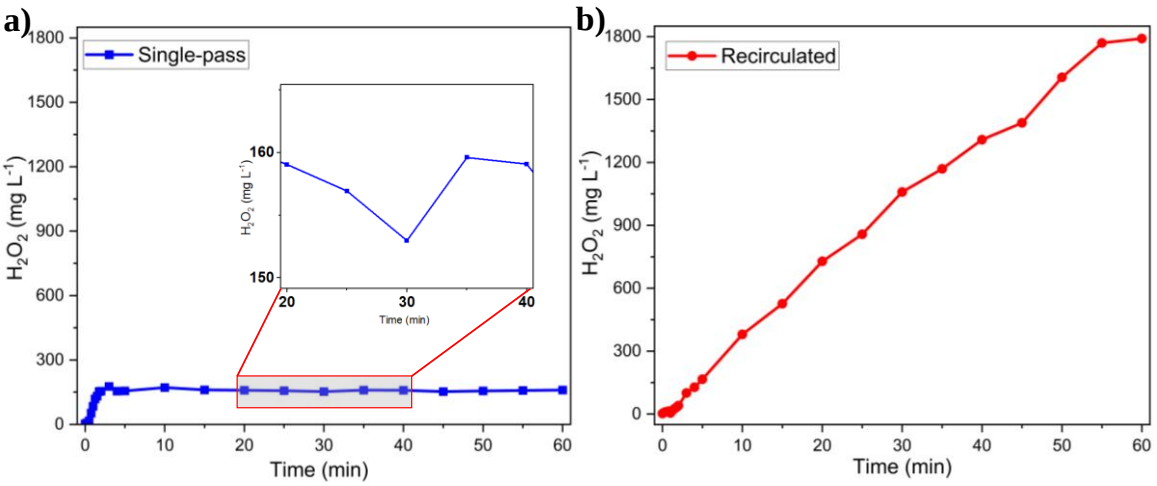

Fig. 8. H_2O_2 electrogeneration over time. **a)** Single-pass system; **Insert a)** magnification of the the curve of H_2O_2 concentration. **b)** Recirculating system. Reaction conditions: current density of 150 $mAcm^{-2}$; 100 mL min^{-1} O_2 flow; 0.1 M of K_2SO_4 employed as supporting electrolyte; 10 mL reactor internal volume; and 15 L h^{-1} of liquid flow rate.

As shown in Fig. 8a, the amount of H_2O_2 produced over time was monitored under the single-pass system. After 2 minutes of electrolysis, the concentration stabilized at approximately 158 mg L^{-1} for the entire duration of the experiment, with a total of 15 L of electrolyte passing through the system. In these conditions, the RSM predicted a H_2O_2 concentration of 162 mg L^{-1}, which was consistent with the experimental results. In contrast, the H_2O_2 concentration profile in the recirculating system (Fig. 8-b) was considerably different from that of the single-pass system, since the accumulation of H_2O_2 occurs in only one liter volume, with the electrolyte recirculating through the EFR about 15 times. The concentration of H_2O_2 increased steadily during the 60 minutes of electrosynthesis, reaching a maximum concentration of 1,780 mg L^{-1}.

For a more accurate comparative analysis of the two systems, we converted the H_2O_2 concentration (in mg L^{-1}) to mass per minute (in units of mg min^{-1}). The results obtained are presented in Table 2. Our findings show that the single-pass system is 32.4% more efficient than the recirculating system in terms of H_2O_2 production and consumes less energy during the process; this outcome can be attributed to the decomposition effect described previously, as the recirculating system makes the electrolyte pass through the reactor repeatedly, at a liquid flow rate of 15 L h^{-1}.

Table 2. Comparison of the single-pass and recirculating systems in terms of H_2O_2 electrogeneration.

System	$[H_2O_2]$ (mg $h^{-1}L^{-1}$)	H_2O_2 (mg min^{-1})	EC (kWh kg^{-1})
Single-pass	2,370	39.5	12.66
Recirculating	1,780	29.6	16.76

While the recirculating system can stimulate the accumulation of hydrogen peroxide in low volumes, the decomposition of the chemical compound can make this mechanism less effective. When it comes to the choice of the system for electrolyses, certain factors need to be considered. For example, in cases where the H_2O_2 is consumed after it is generated - such as in drinking water disinfection [44] or as an oxidant in synthesis [45] - the recirculating system may be more suitable than the single-pass system due to the smaller volume involved in the former. In larger structures, such as wastewater treatment plants, hydrogen peroxide can be applied in tanks with greater volumes for degradation and remediation (as illustrated in the graphical abstract); in such cases, the single-pass system has several advantages, including ease of implementation, maintenance, scale-up, and lower energy consumption.

4 Conclusion and outlook

In this study, we presented a electrochemical flow reactor for *in-situ* H_2O_2 electrogeneration. The effects of hydrodynamic behavior on the EFR were compared by

629 analyzing the response surface graph of flow rate and inter-electrode gap in relation to H_2O_2
630 concentration. Residence time distribution (RTD) was used for the characterization of
631 hydrodynamic behavior in the reactor, and a comparative analysis was performed aiming at
632 comparing H_2O_2 kinetics with the RTD data. The application of a fixed reactor volume (5
633 mL) with a relatively lower RTD (0.28 min) and a higher flow rate (45 L h^{-1}) resulted in the
634 production of low H_2O_2 concentration (9 mg L^{-1}). By contrast, the application of a relatively
635 higher RTD (0.72 min) at a lower flow rate (15 L h^{-1}) led to the production of a relatively
636 higher H_2O_2 concentration (113 mg L^{-1}). The CSTR + PFR model fitted very well with the
637 experimental data, with accurate t_m values which represented the asymmetries of the RTD
638 curves.

639 A response surface methodology (RSM), obtained through the design of experiments,
640 was used to improve our understanding of the system and to model the electrochemical
641 conditions in the GDE-based flow reactor investigated in this study. The RSM-based
642 approach demonstrated the role played by different elements in the electrochemical reactor,
643 and GDE was found to exert a significant effect on current and oxygen conditions,
644 contributing to 78% efficiency for both factors (current and oxygen conditions).
645 Conductivity was found to be the major factor responsible for energy consumption (with
646 values less than 10 kWh kg^{-1} of H_2O_2); this element can be modulated by adjusting the
647 concentration of salts. Furthermore, the RSM can be used to model the conditions of an
648 electrochemical reactor with an equation that predicts efficiency and energy consumption
649 for different H_2O_2 concentrations. This model can be used to modulate the electrolysis
650 conditions in different situations on demand, including low energy cost, high efficiency, and
651 high hydrogen peroxide production.

652 Most studies reported in the literature related to the operational design of
653 electrochemical reactor systems applied for H_2O_2 electrogeneration have employed the

recirculating system for the conduct of electrolyses; this system involves passing a low volume of liquid through the electrochemical reactor multiple times. The major underlying constraint of the recirculating system is that the decomposition of H_2O_2 can make the system less efficient (34% less) compared to the single-pass system, which involves passing the liquid through the reactor only once. The recirculating system is suitable for H_2O_2 accumulation in low volumes, while the single-pass system is more suitable for larger structures such as wastewater treatment plants. In the single-pass system, the electrochemical reactor can be connected in parallel with the liquid phase, producing H_2O_2 that can be used as an oxidant; this system has several advantages, including low energy consumption, easy scalability, and ease of maintenance and implementation.

ACKNOWLEDGEMENTS

The authors are sincerely grateful to Prof. Dr. Edenir Rodrigo Pereira Filho (from Group of Applied Instrumental Analysis, Department of Chemistry, Federal University of São Carlos) for the assistance with the statistical revision. Additionally, we warmly acknowledge the financial assistance provided by the Brazilian research funding agencies, including the Brazilian National Council for Scientific and Technological Development – CNPq (grants #303759/2014-3 and #303943/2021-1), São Paulo Research Foundation - FAPESP (grants #2014/50945-4; #2016/19612-4 and #2017/10118-0), in support of this research.

Declaration of Competing Interest

The authors declare that they have no known competing financial interests or personal relationships that could have appeared to influence the work reported in this paper.

5 References

(1) Ciriminna, R.; Albanese, L.; Meneguzzo, F.; Pagliaro, M. Hydrogen Peroxide: A Key Chemical for Today's Sustainable Development. *ChemSusChem* **2016**, *9* (24), 3374–3381. https://doi.org/https://doi.org/10.1002/cssc.201600895.

(2) Jatta, M.; Kiefer, C.; Patolia, H.; Pan, J.; Harb, C.; Marr, L. C.; Baffoe-Bonnie, A. N95 Reprocessing by Low Temperature Sterilization with 59% Vaporized Hydrogen Peroxide during the 2020 COVID-19 Pandemic. *Am J Infect Control* **2021**, *49* (1), 8–14. https://doi.org/10.1016/j.ajic.2020.06.194.

(3) Pradhan, D.; Biswasroy, P.; Kumar Naik, P.; Ghosh, G.; Rath, G. A Review of Current Interventions for COVID-19 Prevention. *Arch Med Res* **2020**, *51* (5), 363–374. https://doi.org/https://doi.org/10.1016/j.arcmed.2020.04.020.

(4) Gao, G.; Tian, Y.; Gong, X.; Pan, Z.; Yang, K.; Zong, B. Advances in the Production Technology of Hydrogen Peroxide. *Chinese Journal of Catalysis* **2020**, *41* (7), 1039–1047. https://doi.org/https://doi.org/10.1016/S1872-2067(20)63562-8.

(5) Campos-Martin, J. M.; Blanco-Brieva, G.; Fierro, J. L. G. Hydrogen Peroxide Synthesis: An Outlook beyond the Anthraquinone Process. *Angewandte Chemie International Edition* **2006**, *45* (42), 6962–6984. https://doi.org/https://doi.org/10.1002/anie.200503779.

(6) Zhou, W.; Meng, X.; Gao, J.; Alshawabkeh, A. N. Hydrogen Peroxide Generation from O2 Electroreduction for Environmental Remediation: A State-of-the-Art Review. *Chemosphere* **2019**, *225*, 588–607. https://doi.org/https://doi.org/10.1016/j.chemosphere.2019.03.042.

(7) Muddemann, T.; Haupt, D.; Sievers, M.; Kunz, U. Electrochemical Reactors for Wastewater Treatment. *ChemBioEng Reviews* **2019**, *6* (5), 142–156. https://doi.org/https://doi.org/10.1002/cben.201900021.

(8) Al-Amshawee, S. K. A.; Husain, M. S. B.; Yunus, M. Y. B. M.; Mohamed Azmin, N. F.; Temidayo Lekan, O. Extruded and Overlapped Geometries of Feed Spacers for Solution Mixing in Electrochemical Reactors and Electrodialysis-Related Processes. *Chem Eng Commun* **2022**, 1–25. https://doi.org/10.1080/00986445.2022.2042271.

(9) McKerracher, R. D.; Ponce de Leon, C.; Wills, R. G. A.; Shah, A. A.; Walsh, F. C. A Review of the Iron–Air Secondary Battery for Energy Storage. *Chempluschem* **2015**, *80* (2), 323–335. https://doi.org/https://doi.org/10.1002/cplu.201402238.

(10) Perry, S. C.; Ponce de León, C.; Walsh, F. C. Review—The Design, Performance and Continuing Development of Electrochemical Reactors for Clean Electrosynthesis. *J Electrochem Soc* **2020**, *167* (15), 155525. https://doi.org/10.1149/1945-7111/abc58e.

(11) Rivera, F. F.; Pérez, T.; Castañeda, L. F.; Nava, J. L. Mathematical Modeling and Simulation of Electrochemical Reactors: A Critical Review. *Chem Eng Sci* **2021**, *239*, 116622. https://doi.org/https://doi.org/10.1016/j.ces.2021.116622.

(12) Ma, R.; Lin, G.; Zhou, Y.; Liu, Q.; Zhang, T.; Shan, G.; Yang, M.; Wang, J. A Review of Oxygen Reduction Mechanisms for Metal-Free Carbon-Based Electrocatalysts. *NPJ Comput Mater* **2019**, *5* (1), 78. https://doi.org/10.1038/s41524-019-0210-3.

(13) Cornejo, O. M.; Sirés, I.; Nava, J. L. Electrosynthesis of Hydrogen Peroxide Sustained by Anodic Oxygen Evolution in a Flow-through Reactor. *Journal of Electroanalytical Chemistry* **2020**, *873*, 114419. https://doi.org/https://doi.org/10.1016/j.jelechem.2020.114419.

(14) Garg, S.; Li, M.; Weber, A. Z.; Ge, L.; Li, L.; Rudolph, V.; Wang, G.; Rufford, T. E. Advances and Challenges in Electrochemical CO2 Reduction Processes: An Engineering and Design Perspective Looking beyond New Catalyst Materials. *J Mater Chem A Mater* **2020**, *8* (4), 1511–1544. https://doi.org/10.1039/C9TA13298H.

(15) Xie, J.; Jing, J.; Gu, J.; Guo, J.; Li, Y.; Zhou, M. Hydrogen Peroxide Generation from Gas Diffusion Electrode for Electrochemical Degradation of Organic Pollutants in Water: A Review. *J Environ Chem Eng* **2022**, *10* (3), 107882. https://doi.org/https://doi.org/10.1016/j.jece.2022.107882.

(16) Sánchez-Montes, I.; O. S. Santos, G.; O. Silva, T.; Colombo, R.; R. V. Lanza, M. An Innovative Approach to the Application of Electrochemical Processes Based on the In-Situ Generation of H2O2 for Water Treatment. *J Clean Prod* **2023**, *392*, 136242. https://doi.org/https://doi.org/10.1016/j.jclepro.2023.136242.

(17) Carneiro, J. F.; Silva, F. L.; Martins, A. S.; Dias, R. M. P.; Titato, G. M.; Santos-Neto, Á. J.; Bertazzoli, R.; Lanza, M. R. V. Simultaneous Degradation of Hexazinone and Diuron Using ZrO2-Nanostructured Gas Diffusion Electrode. *Chemical Engineering Journal* **2018**, *351*, 650–659. https://doi.org/https://doi.org/10.1016/j.cej.2018.06.122.

(18) Rocha, R. S.; Silva, F. L.; Valim, R. B.; Barros, W. R. P.; Steter, J. R.; Bertazzoli, R.; Lanza, M. R. V. Effect of Fe2+ on the Degradation of the Pesticide Profenofos by Electrogenerated H2O2. *Journal of Electroanalytical Chemistry* **2016**, *783*, 100–105. https://doi.org/https://doi.org/10.1016/j.jelechem.2016.11.038.

(19) Catañeda, L. F.; Rivera, F. F.; Pérez, T.; Nava, J. L. Mathematical Modeling and Simulation of the Reaction Environment in Electrochemical Reactors. *Curr Opin Electrochem* **2019**, *16*, 75–82. https://doi.org/https://doi.org/10.1016/j.coelec.2019.04.025.

(20) Reis, R. M.; Beati, A. A. G. F.; Rocha, R. S.; Assumpção, M. H. M. T.; Santos, M. C.; Bertazzoli, R.; Lanza, M. R. V. Use of Gas Diffusion Electrode for the In Situ Generation of Hydrogen Peroxide in an Electrochemical Flow-By Reactor. *Ind Eng Chem Res* **2012**, *51* (2), 649–654. https://doi.org/10.1021/ie201317u.

(21) Mohaghegh Montazeri, M.; Hejazi, S. A.; Taghipour, F. Multiphysics Modeling of Flow-through Advanced Oxidation Photoreactors with in-Situ Hydrogen Peroxide Electrogeneration. *J Environ Chem Eng* **2023**, *11* (3), 109636. https://doi.org/https://doi.org/10.1016/j.jece.2023.109636.

(22) Fogler, H. S. *Elements of Chemical Reaction Engineering*, 5th ed.; 2016; Vol. 1.

(23) Walker, W. S.; Bezerra Cavalcanti, E.; Atrashkevich, A.; Fajardo, A. S.; Brillas, E.; Garcia-Segura, S. Mass Transfer and Residence Time Distribution in an Electrochemical Cell with an Air-Diffusion Electrode: Effect of Air Pressure and Mesh Promoters. *Electrochim Acta* **2021**, *378*, 138131. https://doi.org/https://doi.org/10.1016/j.electacta.2021.138131.

(24) Oloman, C.; Watkinson, A. P. Hydrogen Peroxide Production in Trickle-Bed Electrochemical Reactors. *J Appl Electrochem* **1979**, *9* (1), 117–123. https://doi.org/10.1007/BF00620593.

(25) Li, Y.; Zhang, Y.; Xia, G.; Zhan, J.; Yu, G.; Wang, Y. Evaluation of the Technoeconomic Feasibility of Electrochemical Hydrogen Peroxide Production for Decentralized Water Treatment. *Front Environ Sci Eng* **2020**, *15* (1), 1. https://doi.org/10.1007/s11783-020-1293-2.

(26) Marques Cordeiro-Junior, P. J.; Sáez Jiménez, C.; Vasconcelos Lanza, M. R. de; Rodrigo Rodrigo, M. A. Electrochemical Production of Extremely High Concentrations of Hydrogen Peroxide in Discontinuous Processes. *Sep Purif Technol* **2022**, *300*, 121847. https://doi.org/https://doi.org/10.1016/j.seppur.2022.121847.

(27) Carneiro, J. F.; Silva, F. L.; Martins, A. S.; Dias, R. M. P.; Titato, G. M.; Santos-Neto, Á. J.; Bertazzoli, R.; Lanza, M. R. V. Simultaneous Degradation of Hexazinone and Diuron Using ZrO2-Nanostructured Gas Diffusion Electrode. *Chemical Engineering Journal* **2018**, *351*, 650–659. https://doi.org/https://doi.org/10.1016/j.cej.2018.06.122.

(28) Levenspiel, O. The Chemical Reactor Omnibook. Oregon State University Book Stores. *Inc., Corvalis, OR* **1989**.

(29) *Design of Experiments for Pharmaceutical Product Development*; Beg, S., Ed.; Springer Singapore: Singapore, 2021. https://doi.org/10.1007/978-981-33-4717-5.

(30) Cornejo, O. M.; Sirés, I.; Nava, J. L. Electrosynthesis of Hydrogen Peroxide Sustained by Anodic Oxygen Evolution in a Flow-through Reactor. *Journal of Electroanalytical Chemistry* **2020**, *873*, 114419. https://doi.org/https://doi.org/10.1016/j.jelechem.2020.114419.

(31) Cordeiro-Junior, P. J. M.; Lobato Bajo, J.; Lanza, M. R. de V.; Rodrigo Rodrigo, M. A. Highly Efficient Electrochemical Production of Hydrogen Peroxide Using the GDE Technology. *Ind Eng Chem Res* **2022**, *61* (30), 10660–10669. https://doi.org/10.1021/acs.iecr.2c01669.

(32) Pérez, J. F.; Sáez, C.; Llanos, J.; Cañizares, P.; López, C.; Rodrigo, M. A. Improving the Efficiency of Carbon Cloth for the Electrogeneration of H2O2: Role of Polytetrafluoroethylene and Carbon Black Loading. *Ind Eng Chem Res* **2017**, *56* (44), 12588–12595. https://doi.org/10.1021/acs.iecr.7b02563.

(33) Peres, J. C. G.; Silvio, U. de; Teixeira, A. C. S. C.; Guardani, R.; Jr., A. dos S. V. Study of an Annular Photoreactor with Tangential Inlet and Outlet: I. Fluid Dynamics. *Chem Eng Technol* **2015**, *38* (2), 311–318. https://doi.org/https://doi.org/10.1002/ceat.201400186.

(34) Cordeiro-Junior, P. J. M.; Lobato Bajo, J.; Lanza, M. R. de V.; Rodrigo Rodrigo, M. A. Highly Efficient Electrochemical Production of Hydrogen Peroxide Using the GDE Technology. *Ind Eng Chem Res* **2022**, *61* (30), 10660–10669. https://doi.org/10.1021/acs.iecr.2c01669.

(35) Oloman, C.; Watkinson, A. P. Hydrogen Peroxide Production in Trickle-Bed Electrochemical Reactors. *J Appl Electrochem* **1979**, *9* (1), 117–123. https://doi.org/10.1007/BF00620593.

(36) Li, Y.; Zhang, Y.; Xia, G.; Zhan, J.; Yu, G.; Wang, Y. Evaluation of the Technoeconomic Feasibility of Electrochemical Hydrogen Peroxide Production for Decentralized Water Treatment. *Front Environ Sci Eng* **2020**, *15* (1), 1. https://doi.org/10.1007/s11783-020-1293-2.

(37) Zhang, Q.; Zhou, M.; Ren, G.; Li, Y.; Li, Y.; Du, X. Highly Efficient Electrosynthesis of Hydrogen Peroxide on a Superhydrophobic Three-Phase Interface by Natural Air Diffusion. *Nat Commun* **2020**, *11* (1), 1731. https://doi.org/10.1038/s41467-020-15597-y.

(38) Moreira, J.; Bocalon Lima, V.; Athie Goulart, L.; Lanza, M. R. V. Electrosynthesis of Hydrogen Peroxide Using Modified Gas Diffusion Electrodes (MGDE) for Environmental Applications: Quinones and Azo Compounds Employed as Redox Modifiers. *Appl Catal B* **2019**, *248*, 95–107. https://doi.org/https://doi.org/10.1016/j.apcatb.2019.01.071.

(39) Cordeiro-Junior, P. J. M.; Martins, A. S.; Pereira, G. B. S.; Rocha, F. V.; Rodrigo, M. A. R.; Lanza, M. R. de V. Bisphenol-S Removal via Photoelectro-Fenton/H2O2 Process Using Co-Porphyrin/Printex L6 Gas Diffusion Electrode. *Sep Purif Technol* **2022**, *285*, 120299. https://doi.org/https://doi.org/10.1016/j.seppur.2021.120299.

(40) Xia, Y.; Shang, H.; Zhang, Q.; Zhou, Y.; Hu, X. Electrogeneration of Hydrogen Peroxide Using Phosphorus-Doped Carbon Nanotubes Gas Diffusion Electrodes and Its Application in Electro-Fenton. *Journal of Electroanalytical Chemistry* **2019**, *840*, 400–408. https://doi.org/https://doi.org/10.1016/j.jelechem.2019.04.009.

(41) Wang, W.; Lu, X.; Su, P.; Li, Y.; Cai, J.; Zhang, Q.; Zhou, M.; Arotiba, O. Enhancement of Hydrogen Peroxide Production by Electrochemical Reduction of Oxygen on Carbon Nanotubes Modified with Fluorine. *Chemosphere* **2020**, *259*, 127423. https://doi.org/https://doi.org/10.1016/j.chemosphere.2020.127423.

(42) Xia, G.; Lu, Y.; Xu, H. An Energy-Saving Production of Hydrogen Peroxide via Oxygen Reduction for Electro-Fenton Using Electrochemically Modified Polyacrylonitrile-Based Carbon Fiber Brush Cathode. *Sep Purif Technol* **2015**, *156*, 553–560. https://doi.org/https://doi.org/10.1016/j.seppur.2015.10.048.

(43) Sahinkaya, E.; Tuncman, S.; Koc, I.; Guner, A. R.; Ciftci, S.; Aygun, A.; Sengul, S. Performance of a Pilot-Scale Reverse Osmosis Process for Water Recovery from Biologically-Treated Textile Wastewater. *J Environ Manage* **2019**, *249*, 109382. https://doi.org/https://doi.org/10.1016/j.jenvman.2019.109382.

(44) Jin, Y.; Shi, Y.; Chen, Z.; Chen, R.; Chen, X.; Zheng, X.; Liu, Y. Combination of Sunlight with Hydrogen Peroxide Generated at a Modified Reticulated Vitreous Carbon for Drinking Water Disinfection. *J Clean Prod* **2020**, *252*, 119794. https://doi.org/https://doi.org/10.1016/j.jclepro.2019.119794.

(45) Lyu, J.; Niu, L.; Shen, F.; Wei, J.; Xiang, Y.; Yu, Z.; Zhang, G.; Ding, C.; Huang, Y.; Li, X. In Situ Hydrogen Peroxide Production for Selective Oxidation of Benzyl Alcohol over a Pd@Hierarchical Titanium Silicalite Catalyst. *ACS Omega* **2020**, *5* (27), 16865–16874. https://doi.org/10.1021/acsomega.0c02065.